Surface & Coatings Technology 344 (2018) 373–382

Contents lists available at ScienceDirect

Surface & Coatings Technology

journal homepage: www.elsevier.com/locate/surfcoat

Growth mechanisms of Ca- and P-rich MAO films in Ti-15Zr-xMo alloys for osseointegrative implants

D.R.N. Correa[a,b,*], L.A. Rocha[a,c], A.R. Ribeiro[a,d,e], S. Gemini-Piperni[g], B.S. Archanjo[f], C.A. Achete[f], J. Werckmann[g], C.R.M. Afonso[h], M. Shimabukuro[i], H. Doi[j], Y. Tsutsumi[j,k], T. Hanawa[j]

[a] IBTN/BR – Brazilian Branch Institute of Biomaterials, Tribocorrosion and Nanomedicine, Bauru, SP, Brazil
[b] IFSP – Federal Institute of Education, Science and Technology, Sorocaba, SP, Brazil
[c] UNESP – Univ Estadual Paulista, Laboratório de Anelasticidade e Biomateriais, Bauru, SP, Brazil
[d] Postgraduate Program in Biotechnology, National Institute of Metrology, Quality and Technology, 25250-020 Duque de Caxias, RJ, Brazil
[e] UNIGRANRIO - University of Grande Rio, Post-Graduate Program on Translational Biomedicine, Duque de Caxias, RJ, Brazil
[f] INMETRO - National Institute of Metrology Quality and Technology, Metrology Materials Division, Duque de Caxias, RJ, Brazil
[g] CBPF – Centro Brasileiro de Pesquisas Físicas, Rio de Janeiro, RJ, Brazil
[h] UFSCar – Federal University of São Carlos, Department of Materials Engineering, São Carlos, SP, Brazil
[i] TMDU - Tokyo Medical and Dental University, Graduate School of Medical and Dental Sciences, Tokyo, Japan
[j] TMDU - Tokyo Medical and Dental University, Institute of Biomaterials and Bioengineering, Tokyo, Japan
[k] The University of Tokyo, Graduate School of Engineering, Tokyo, Japan

ARTICLE INFO

Keywords:
Ti-Zr-Mo alloy
Micro-arc oxidation
Crystalline structure
Bioactivity
Mineralization

ABSTRACT

In this study, a micro-arc oxidation treatment was applied to Ti-15Zr-xMo (x = 0, 5, 10 and 15 wt%) alloys to produce porous oxide layers enriched with bioactive ions (calcium and phosphorus) for use as osseointegrative implants. Biocompatibility studies, namely metabolic activity, mineralization and differentiation studies were conducted with human osteoblastic cell line SAOS-2. A typical porous coating was obtained in all samples, with similar morphologies and thicknesses, which were found to be dependent on the maximum applied voltage. Calcium and phosphorus ions were incorporated into the films, as indicated by EDX analysis. Chemical analyses indicated that the films were composed preferentially of Ti and Zr oxides. XRD patterns revealed mostly substrate Ti phases. However, cross-sectional TEM imaging and automated phase and orientation mapping showed distinct amorphous and nanocrystalline regions within the films, with a higher fraction of Ca atoms incorporated in the outer layer. After immersion in Hanks' Balanced Salt Solution (HBSS) for seven days, small amounts of calcium phosphate precipitates were observed at the surface of all samples which were confirmed by ICP-AES measurements, indicating that the MAO treatment possibly introduced a considerable bioactive response in the samples. Biological results indicate that Ti-15Zr-15Mo MAO-treated surfaces are biocompatible and induce a higher osteoblasts viability and mineralization. The combination of porous structure and bioactive composition of the oxide layers can be suitable for use as advanced biomedical implants with osseointegration ability.

1. Introduction

Titanium (Ti) and its alloys have been successfully employed as load-bearing implants, where biocompatibility, osseointegration and bioactivity are important factors to be considered jointly with mechanical and tribocorrosion properties [1]. In comparison with commonly used Co-Cr-Mo alloys and 316 L type stainless steel, Ti-based alloys displays a special combination of high strength-to-density ratio, excellent corrosion resistance, relatively low Young's modulus and recognized biocompatibility for most applications [2]. Ti-15Zr-based alloys with different molybdenum (Mo) contents have been recently developed to ensure Young's modulus close to the human bone (to prevent the stress shielding effect), and with Al- and V-free composition (to avoid toxic and allergic effects) [3]. Our preliminary results also showed that good tribocorrosion resistance was also achieved in these alloys [4].

Surface modification techniques may be used to change the interaction of Ti-based materials with adjacent bone tissues and to shorten osseointegration time [5,6]. Micro-arc oxidation (MAO) is a low-cost electrochemical treatment which has been applied to valve metals, such

* Corresponding author at: IFSP - Federal Institute of Education, Science and Technology, Sorocaba, SP, Brazil.
E-mail address: diego.correa@ifsp.edu.br (D.R.N. Correa).

https://doi.org/10.1016/j.surfcoat.2018.02.099
Received 5 September 2017; Received in revised form 26 February 2018; Accepted 27 February 2018
Available online 08 March 2018

as Ti, Zr, Ta and Nb. During the treatment, the metallic surface is kept in anodic conditions, above the dielectric breakdown barrier, promoting plasma sparking at the interface metal-electrolyte. Plasma sparking and oxidation reactions can generate a thick porous oxide film which is strongly bonded to the substrate [7,8]. By the manipulation of the electrolyte composition, it is also possible to incorporate ions into the films during plasma sparking [9,10]. Recent developments on surface modification have focused on the establishment of a bioactive response in biomedical metallic surfaces, to induce faster bone regeneration and to repair damaged tissues. Calcium (Ca) and phosphorus (P) are key elements to promote calcium phosphate precipitation around the implant, because they are main elements of the human bone composition [11]. MAO treatments have been applied to Ti surfaces targeting an improvement of its bioactive and osseointegrative responses through the formation of a Ca- and P-rich oxide film [1,6]. Recently, Krzakala et al. [12], Kazek-Kesik et al. [12,13] and Tsutsumi et al. [14] have obtained noticeable improvements of hard-tissue compatibility in some commercial Ti-based alloys by using MAO treatment. Furthermore, MAO-treated Ti surfaces have also exhibited better tribocorrosion resistance, avoiding the release of potential harmful debris from the implant surface to the human body, as reported by Alves et al. [10], Oliveira et al. [8] and Felgueiras et al. [15].

Considering the actual importance of the surface modification for biomedical implants, the aim of this research was to investigate, for the first time, the growth mechanisms and bioactivity of Ca- and P-rich MAO-treated surfaces of Ti-15Zr-based alloys for osseointegrative implants applications. For this purpose, disk-shaped Ti-15Zr-xMo (0, 5, 10 and 15 wt%) alloys were submitted to MAO treatment in an electrolyte containing calcium and phosphorus ions. After that, the morphology, thickness, composition, crystalline structure, calcium phosphate formation capability of the oxide films and biocompatibility were evaluated and related with the MAO experimental parameters and alloy's composition.

2. Materials and methods

2.1. Samples processing

Ingots of Ti-15Zr-xMo (0, 5, 10 and 15 wt%) alloys were produced in an argon arc-melting furnace (AD TAC 501D, Diavac Ltd., Tokyo, Japan) from commercially pure Ti (cp-Ti; Grade 2), pure Zr (99.5%), and pure Mo (99.9%). The metals were re-melted 10 times to ensure homogeneity. Chemical composition of the samples is shown in Table 1, the results were obtained by X-ray fluorescence spectrometry (XRF; XGT-1000WR, Horiba Ltd., Kyoto, Japan) and infrared absorption (LECO TC-400). The materials were cast into rod shape using a centrifugal casting machine (MSE-50TMD-Z, Yoshida Cast Industry Co., Ltd., Saitama, Japan). Disk-type samples (8 mm ϕ × 1.5 mm) were obtained after cut the rod in a water-cooled cutting wheel. Prior to the surface treatment, the samples were polished with waterproof SiC abrasive paper up to #800, ultrasonically washed in acetone and ethanol, and dried in a stream of nitrogen gas. The samples were kept in a desiccator prior to conducting the experiments.

2.2. MAO treatment

For surface modification, the disks were fixed in a polytetrafluorethylene holder with an O-ring. This working electrode followed the specifications described elsewhere [16]. The sample was used as positive electrode (anode) and an ASTM 304 stainless steel plate was used as cathode. A DC power supply (PL-650-0.1, Matsusada Precision Inc., Shiga, Japan) was used in galvanostatic mode, with a current density of 311 A/m^2. The maximum voltage was limited to 300 V, 350 V and 400 V, and in all cases the anodic treatments were carried out for 10 min. Electrolyte was composed by 0.15 mol/l calcium acetate ($Ca(CH_3COO)_2$) and 0.10 mol/l calcium glicerophosphate ($C_3H_7CaO_6P$), based on previous studies [17,18]. During the treatment, the electrolyte solution was agitated by a magnetic stirrer and the glass container was kept in a water-cooled bath at room temperature. The experiments were conducted in triplicate for all samples.

2.3. Surface characterization

Surface and cross-section of the MAO films were analyzed by scanning electron microscopy (SEM; S-3400NX, Hitachi High-Technologies Corp., Tokyo, Japan), coupled with energy dispersive X-ray spectroscopy (EDX), and transmission electron microscopy (TEM; Titan FEI microscope at 300 kV, coupled with EDX detector). For TEM analysis, thin foils of the cross-section area were obtained by dual beam Quanta 3S SEM equipment. Automated phase and orientation mapping (ACOM-TEM) was made by Astar package, using crystallographical sheets of TiO_2 (anatase (n. 1526931) and rutile (n. 1534781)) and bulk Ti phases (α (n. 43416) and β (n. 44391)). Phase compositions were evaluated by X-ray diffraction measurements (XRD; D8 Discover, Bruker Corp., Yokohama, Japan), Ni-filtered CuK_α radiation (λ = 0.1544 nm), at 40 mA, 40 kV, and step size of 0.08° s^{-1}.

2.4. Bioactivity evaluation

Assaying by immersion in Hanks' Balanced Salt Solution (HBSS) solution was performed to evaluate preliminarily the bioactive response of the MAO films. Hanks' solution, without glucose, was produced from commercial grade pure reagents, and the pH was adjusted to 7.4. Main composition of the Hanks' solution is shown in Table 2. Samples were kept inside of perfluoroalkoxy alkane bottles with 15 ml of solution, at 37 °C during 7 days. Prior to the experiments, the bottles were washed with nitric acid and ultra-pure water. Investigation of the surface morphology after immersion was carried out by SEM. Amount of calcium and phosphate ions were quantified by inductively coupled plasma atomic spectrometer (ICP-AES: ICPS-7000 ver. 2, Shimadzu Corp., Kyoto, Japan). The precipitates were dissolved by soaking the samples in nitric acid and pure water solution (1:99). Standard solutions with calcium and phosphate ions (0.01, 0.1 and 1 ppm) were made as standards. CP-Ti and pure Zr were used as comparisons. The tests were made in triplicate for each sample.

2.5. Cell culture

20,000 cell/well were plated on Ti-15Zr-15Mo and MAO-treated Ti-15Zr-15Mo (400 V) respectively in high glucose-Dulbecco's Modified

Table 1
Chemical composition of the alloys employed in this study.

Alloy	Ti (wt%)	Zr (wt%)	Mo (wt%)	Fe, Cr, Sn and Hf (wt%)	N (ppm)	O (ppm)	H (ppm)
Ti-15Zr	84.46 ± 0.09	15.28 ± 0.07	0.08 ± 0.03	< 1	< 100	< 1000	< 50
Ti-15Zr-5Mo	78.85 ± 0.08	15.62 ± 0.08	5.41 ± 0.04				
Ti-15Zr-10Mo	75.23 ± 0.05	15.03 ± 0.09	9.63 ± 0.07				
Ti-15Zr-15Mo	69.07 ± 0.09	15.60 ± 0.07	15.19 ± 0.07				

Table 2
Composition of Hanks' solution (mol/L).

Na^+	K^+	Mg^{2+}	Ca^{2+}	Cl^-	HPO_4^{2-}	SO_4^{2-}	HCO_3^{2-}
$1.42\ 10^{-1}$	$5.81\ 10^{-3}$	$8.11\ 10^{-4}$	$1.26\ 10^{-3}$	$1.45\ 10^{-1}$	$7.78\ 10^{-4}$	$1.261\ 10^{-3}$	$4.17\ 10^{-3}$

Eagle Medium (DMEM) supplemented with 10% fetal bovine serum (FBS), 1% penicillin-streptomycin, 10 μM β-glycerophosphate and 0.05 mg/ml ascorbic acid (osteogenic medium).

2.6. Viability assay

The viability of cells after 1 and 7 days, was determined using the standard MTT [3-(4,5-dimethylthiazol-2-yl)-2,5-diphenyltetrazolium bromide] assay. The purple formazan crystals were dissolved in dimethyl sulfoxide (DMSO), transferred in a 96 well plate (100 μl/well), and the absorbance recorded on a microplate reader at a wavelength of 570 nm with blank subtraction at 690 nm.

2.7. Alkaline phosphatase staining

After 7 and 21 days, the cells were fixed in 4% paraformaldehyde for 10 min, and then washed with PBS. Histochemical evaluation of ALP activity was performed using the Sigma-Aldrich kit n. 85, according to the manufacturer's instruction. ALP staining was dissolved in DMSO, transferred in a 96 well plate (100 μl/well), and the absorbance was recorded on a microplate reader at a wavelength of 570 nm with blank subtraction at 690 nm.

2.8. Alizarin red staining

After 7 and 21 days, the cells were fixed in 4% paraformaldehyde for 10 min, and then washed with PBS. To evaluate mineralization, alizarin red staining was performed. Fixed cells were incubated with 1% alizarin red solution for 30 min, then washed in distillated water. Alizarin red staining was dissolved in solution 0.5 M HCl, 5% sodium dodecyl sulfate (SDS) (100 μl/well), transferred to a 96 well plate, and the absorbance was recorded on a microplate reader at a wavelength of 415 nm with blank subtraction at 690 nm.

3. Results and discussion

Morphological and cross-sectional images of the MAO films in the Ti-15Zr alloy are displayed in Fig. 1. Identical results were obtained for the other samples. A typical porous structure was found, whereby the pore size clearly was dependent on the limiting voltage. Average pore size tended to increase with the limiting voltage, as shown in Fig. 2a. Average pore size on the outer layer remained in the range of 1.6–1.8 μm for 300 V, 2.2–2.8 μm for 350 V, and 2.8–4.5 μm for 400 V. As evident in Fig. 2a, an increase in the Mo content resulted in an increment of the average pore size.

Film thickness (Fig. 2b) was found to be between 3 and 4 μm for 300 V, 6–8 μm for 350 V, and 8–14 μm for 400 V. No significant effect could be detected between the Mo content and film thickness. In fact, as depicted in Fig. 2b, a gradual increase in the film thickness as a function of the amount of Mo could be observed in the samples prepared at 300 V, while a non-linear dependence was noted at 350 V and 400 V. It is interesting to highlight that the thickness of the anodic film on Ti-15Zr-10Mo alloy appeared to be less dependent on the limited voltage. This aspect will be further investigated in detail in future studies.

During the anodic treatment, there is a combined effect of oxide layer growth and energetic plasma sparking along the surface. Therefore, the pore size and thickness of the MAO-treated surfaces are expected to be directly dependent of the applied voltage, as this favors oxidation reactions and increase plasma sparking energy [7,8]. As comparison, Chen et al. [19] observed a linear increase of the thickness and porous size in Ti-13Cr-3Al-1Fe alloy after MAO treatment in NaH_2PO_4 at voltages between 300 V and 450 V, prepared under potentiostatic conditions. The alloy composition also plays an important role in this process, by changing the dielectric breakdown barrier of the oxide layer. Mo and Zr are alloying elements which improve the corrosion resistance of Ti alloys, as reported recently by Zhou and Luo [20] and Han et al. [21]. However, it appears that these elements have distinct effects on the dielectric barrier of the films when kept in anodic voltages. This assumption is being the scope of further investigation.

Phase composition of the MAO films are shown by the XRD patterns of the Fig. 3. It is possible to identify predominantly peaks from the bulk Ti phases, as hcp (α′ phase), orthorhombic (α″ phase) and bcc (β phase). Intensity of the peaks slightly decreased with the limiting voltage, which can be related with the oxide layer growth. Absence of diffraction peaks from oxide compounds (TiO_2 and ZrO_2), besides thicknesses remained in the order of micrometers, indicates that the MAO films has low crystallinity, which could be a result of the abrupt increase of local temperature and pressure along the surface during plasma sparking and the subsequent very high cooling rate [6]. Yang et al. [22] detected rutile instead of anatase phase on Ti surfaces when the applied voltage increased from 90 V to 180 V, during anodic oxidation in 1 M H_2SO_4 for 1 min. However, Sowa et al. [11] observed a similar lack of crystallinity in Ti-13Nb-13Zr alloy when submitted to MAO treatment in $Ca(H_2PO_2)_2$ and H_3PO_4 solution at a high voltage of 400 V.

TEM analyses were performed on cross-sectioned samples to evaluate the crystallographic aspects of the oxide layers. Data from the MAO-treated Ti-15Zr-5Mo and Ti-15Zr-15Mo alloys, collected at 400 V, were used to evaluate the influence of the substrate's composition and structure on the oxide layer growth, once the alloys displayed α″ + β and β structures, respectively. Cross-sectional TEM images of the MAO film in the Ti-15Zr-5Mo alloy, produced with a limiting voltage of 400 V, are displayed in Fig. 4. In Fig. 4a, three distinct regions can be discerned in the film, having differing thicknesses: an amorphous inner layer (I) of approximately 0.47 μm, a nanocrystalline layer (II) close to 3.00 μm, and a large porous amorphous layer (III) > 11 μm. Selected area electron diffraction (SAED) patterns in Fig. 4b confirmed the structural characteristics identified above: Regions I and III do not display diffraction spots, but Region II demonstrates multiple spots of nanocrystalline oxide phases. A high-resolution TEM (HRTEM) view of the nanocrystalline region (Fig. 4c) shows that the nanograins presented different plane orientations throughout the MAO film. The dense inner layer (I) might have been generated by the growth of the native passive film in the moments before the anodization process. Conversely, the nanocrystalline layer (II) was probably created by the oxidation reactions occurring in the first seconds of the process. The outer layer (III) might have been formed during highly energetic plasma sparking, which produces an aggressive environment with locally high temperatures and pressures, followed by very fast cooling, favoring the growth of a porous amorphous layer. These different layers were observed by Oliveira et al. [8] and Ribeiro et al. [9] in MAO films formed on pure titanium. They observed a similar crystalline composition in MAO films grown in cp-Ti at 300 V for 1 min. The inner layer was composed primarily of anatase, while the top layer exhibited a large quantity of an amorphous phase combined with increasing amounts of rutile. The amorphous layer, rich in Ca, promoted improvement of cell viability and metabolic activity of fibroblasts, in addition to high surface adhesion of osteoblasts [9]. In fact, the semi-quantitative chemical microanalysis of the MAO films (Fig. 4d) revealed that the Ca/Ti ratio increased dramatically in the amorphous outer layer (III), while the Zr/Ti and Mo/Ti ratios remained constant. P atoms were not quantified due to the proximity between the $P_{K\alpha}$ (2013 eV) and the $Zr_{L\alpha}$ (2042 eV) peaks in the EDS spectrum. The superior Zr/Ti ratio compared to the Mo/Ti ratio is a result of the higher stability of Ti and Zr oxides

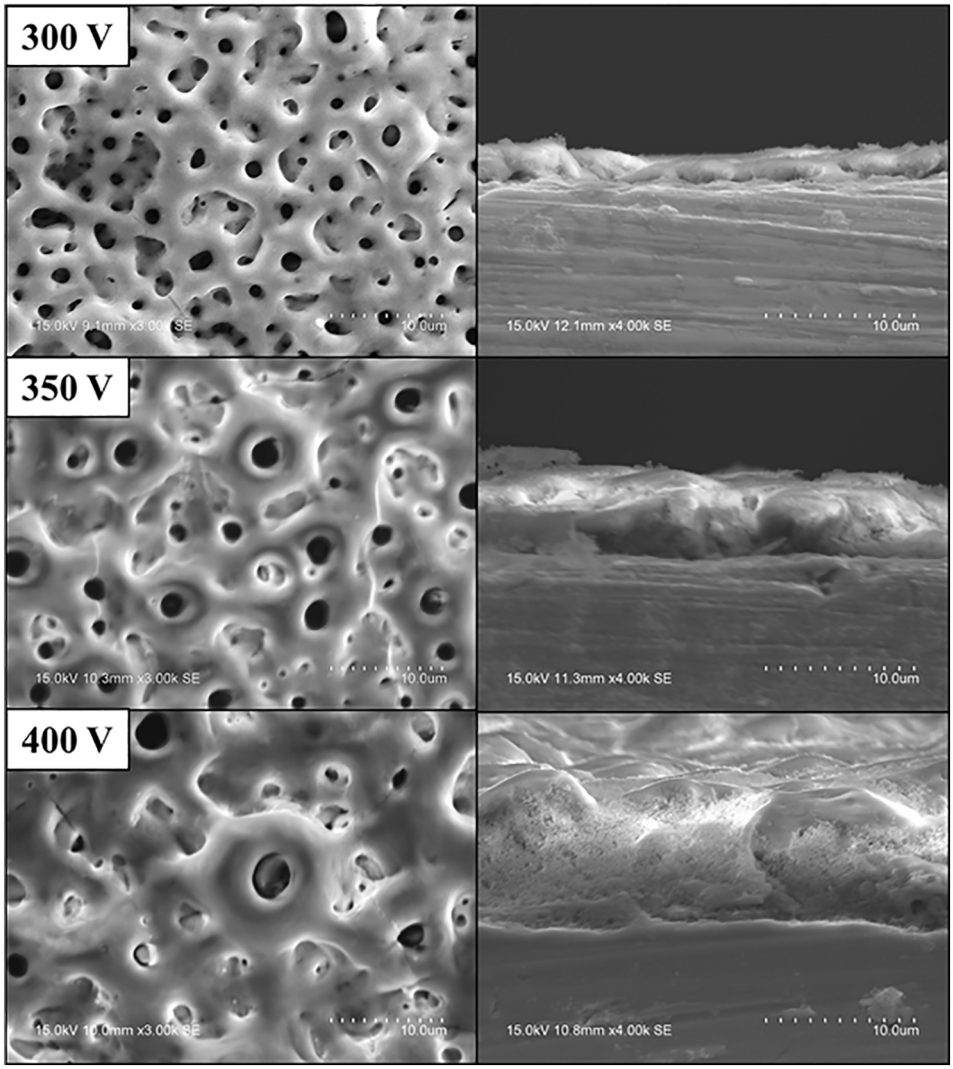

Fig. 1. Morphology and cross-section of MAO-treated Ti-15Zr alloy.

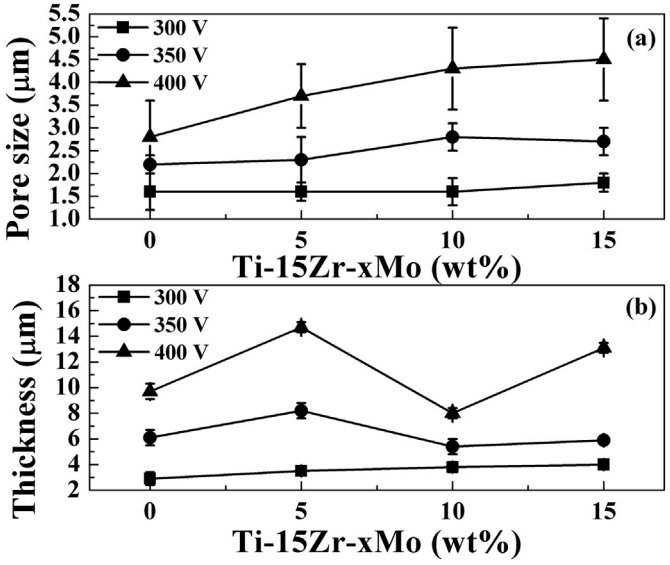

Fig. 2. Pore size (a) and thickness (b) of the MAO films in Ti-15Zr-xMo alloys.

(commonly TiO_2 and ZrO_2), which are more stable than Mo oxides (primarily MoO_3). In terms of the standard Gibbs free energy for metallic oxidation, the ZrO_2 reaction value is −1080 kJ/mol, while TiO_2 reaction value is −945 kJ/mol; both lower than the MoO_3 reaction value (−745 kJ/mol) [23,24]. Mixed TiO_2 and ZrO_2 films were observed in a Ti-50Zr alloy after anodization at 8 V in acidic solutions by Ferreira et al. [25]. Similarly, Simka et al. [26] studied the effect of MAO treatment in a commercial biomedical Ti-15Mo alloy under different applied voltages and electrolyte compositions. X-ray fluorescence (XRF) and X-ray photoelectron spectroscopy (XPS) results indicated that the oxide layer was composed preferentially of TiO_2. These results also show that Ca atoms, and presumably, P atoms, are located primarily in the outer layer, which could be useful for interaction with surrounding bone tissues during implantation, as highlighted by Ribeiro et al. [9]. Identical results found for the MAO film of the Ti-15Zr-15Mo alloy were produced with a limiting voltage of 400 V.

In Fig. 5, ASTAR maps for the MAO film growth in the Ti-15Zr-15Mo alloy grown with a limiting voltage of 400 V are presented. In the virtual bright field (VBF) image (Fig. 5a) a smooth layer (~150 nm) above the substrate (between the dashed lines) is observed which corresponds to the amorphous region I. Above the dashed lines the nanocrystalline region II is present. At the top of the image, the same smooth layer related to the amorphous phase (region III) can be observed. The lack of contrast in the smooth region is a characteristic of amorphous phases, which have homogeneous compositional structure at the nanoscale [27]. In Fig. 5b and c, the index and reliability images, respectively, are presented, which are related to the index quality of the

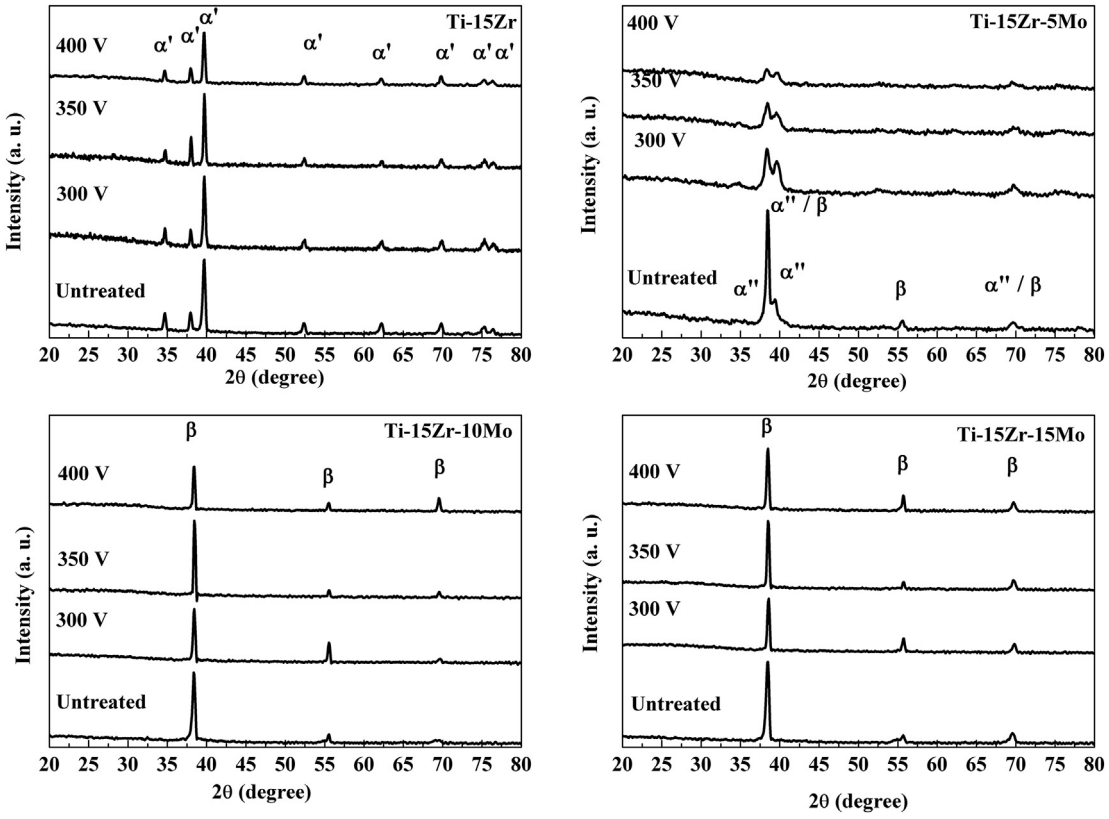

Fig. 3. XRD patterns of MAO-treated samples.

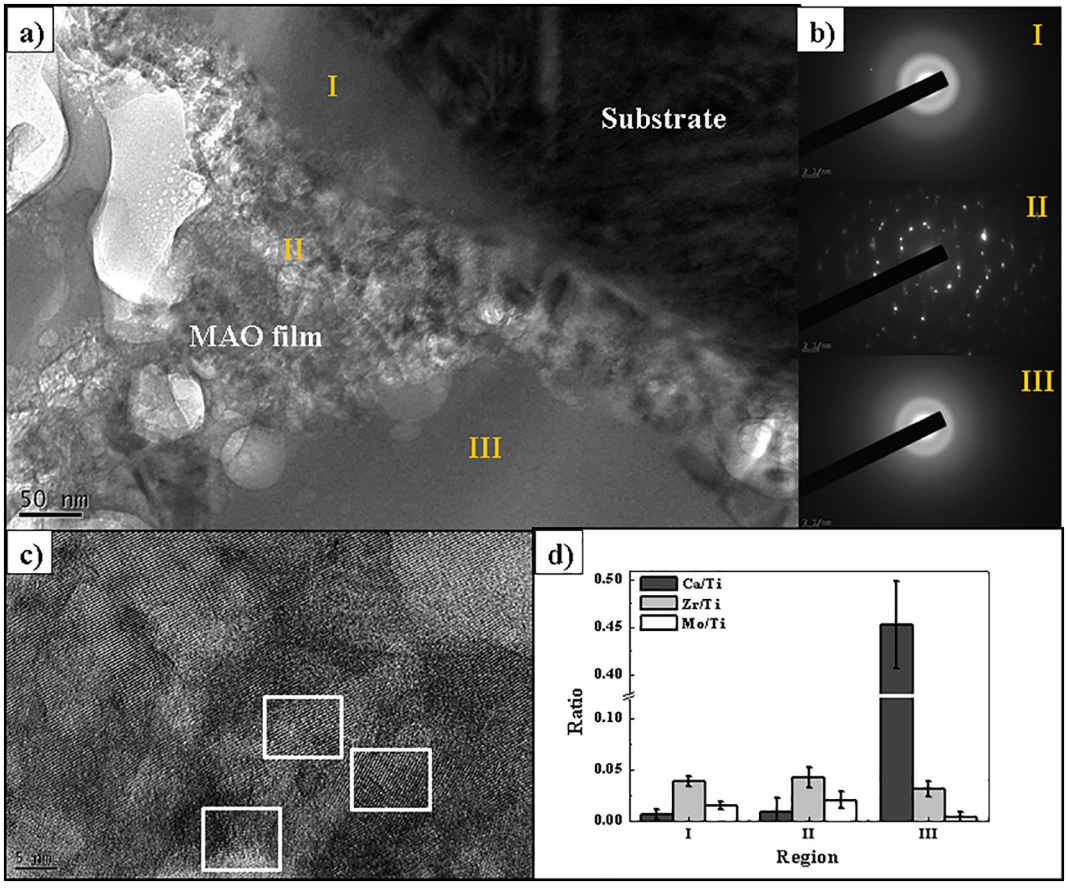

Fig. 4. TEM analysis of MAO-treated Ti-15Zr-5Mo alloy at 400 V: a) Interface film-substrate; b) SAED patterns of the distinct regions of the film; c) HRTEM of the nanocrystalline region of the film; d) chemical ratio of the elements along the film.

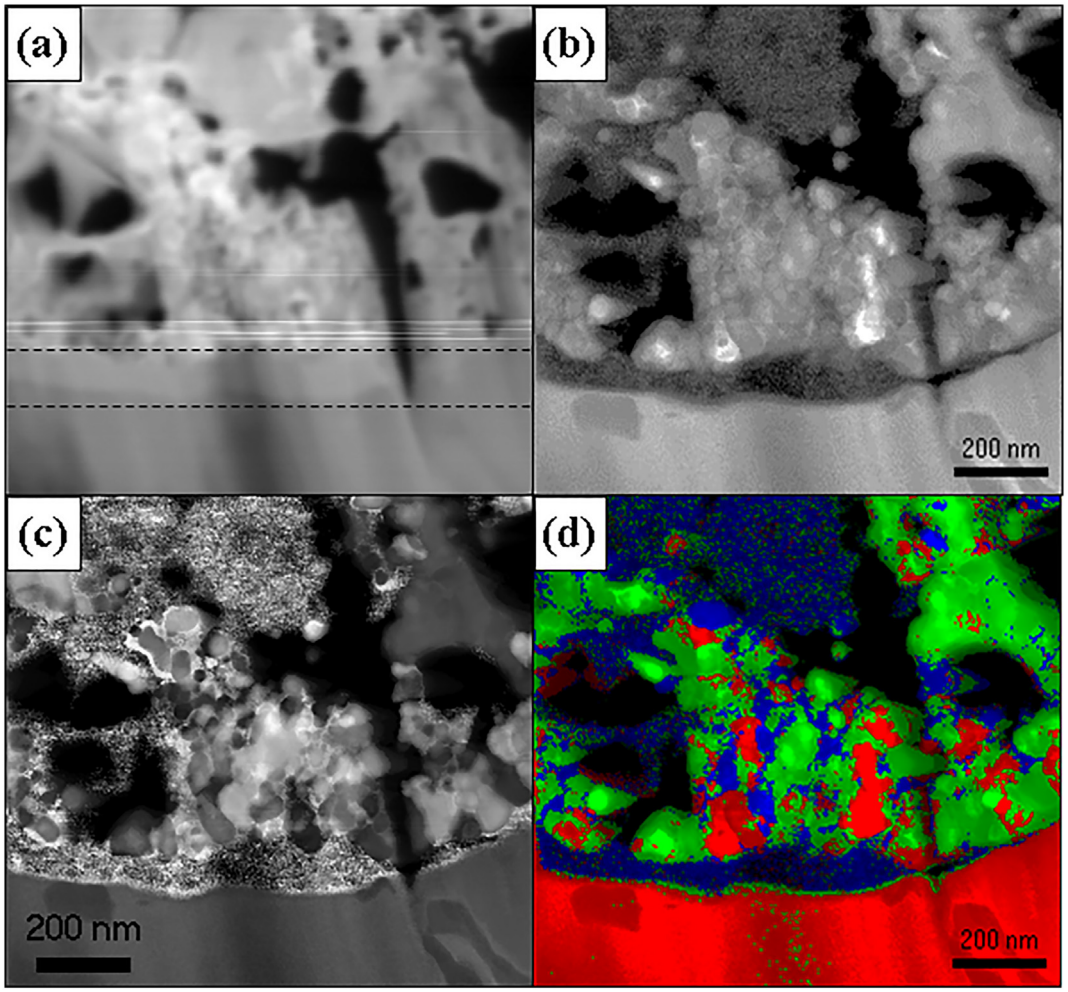

Fig. 5. ASTAR analysis of Ti-15Zr-15Mo alloy: a) virtual bright field (VBF) micrograph, b) Index image, c) Reliability, d) phases (red: β-Ti matrix, green: anatase TiO_2, blue: rutile TiO_2), f) mixed image of phases and index. (For interpretation of the references to colour in this figure legend, the reader is referred to the web version of this article.)

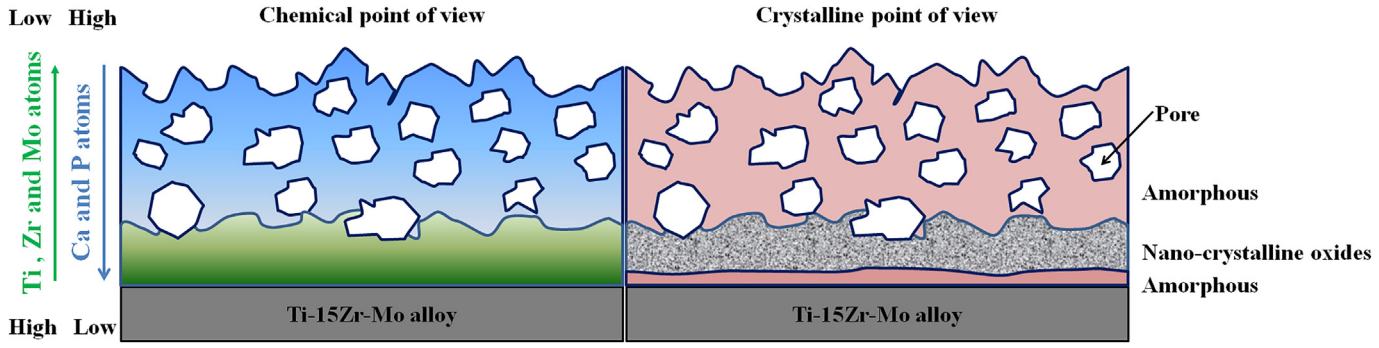

Fig. 6. Schematic view of the chemical and crystalline aspects of the MAO films in the alloys.

phases. In the images, the region II is characterized by nanocrystalline grains of oxide phases (~10 nm) with one gray-scale (globular and spherical shapes), while amorphous phase is denoted with noisy multiple shades of gray scale due to the random orientation of the clustered short-range order (SRO) structure. In Fig. 5d, the superimposed image of oxides and bulk Ti phases is shown. The major part of the nanocrystalline region is composed of the anatase phase, with traces of the rutile phase demonstrated preferentially at the top of the image. Because the amorphous phase lacks crystallinity, its SAED pattern displays only a central halo without diffraction spots. However, the position of this central halo is near the central spot of the TiO_2 phases, which allows the amorphous region to be indexed as a random mixture of anatase and rutile phases. In addition, some spots of the β-Ti phase were identified in the film, as a result of the similar group of orientations between oxide phases and the bcc structure. Besides this, the mixed image fits well with results obtained by Ribeiro et al. [9]. Similar results were obtained for MAO film grown in the Ti-15Zr-5Mo alloy with a limiting voltage of 400 V.

From the results presented here, and based on the results of Ribeiro et al. [9] and Oliveira et al. [8] obtained for cp-Ti, it is possible to draw a schematic view for MAO film grown in Ti-15Zr-Mo alloys (Fig. 6). From the chemical point of view, the outer layer of the film is enriched with Ca and P atoms, being gradually depleted down to the substrate. The film is mostly composed of titanium oxides, with low amount of Zr,

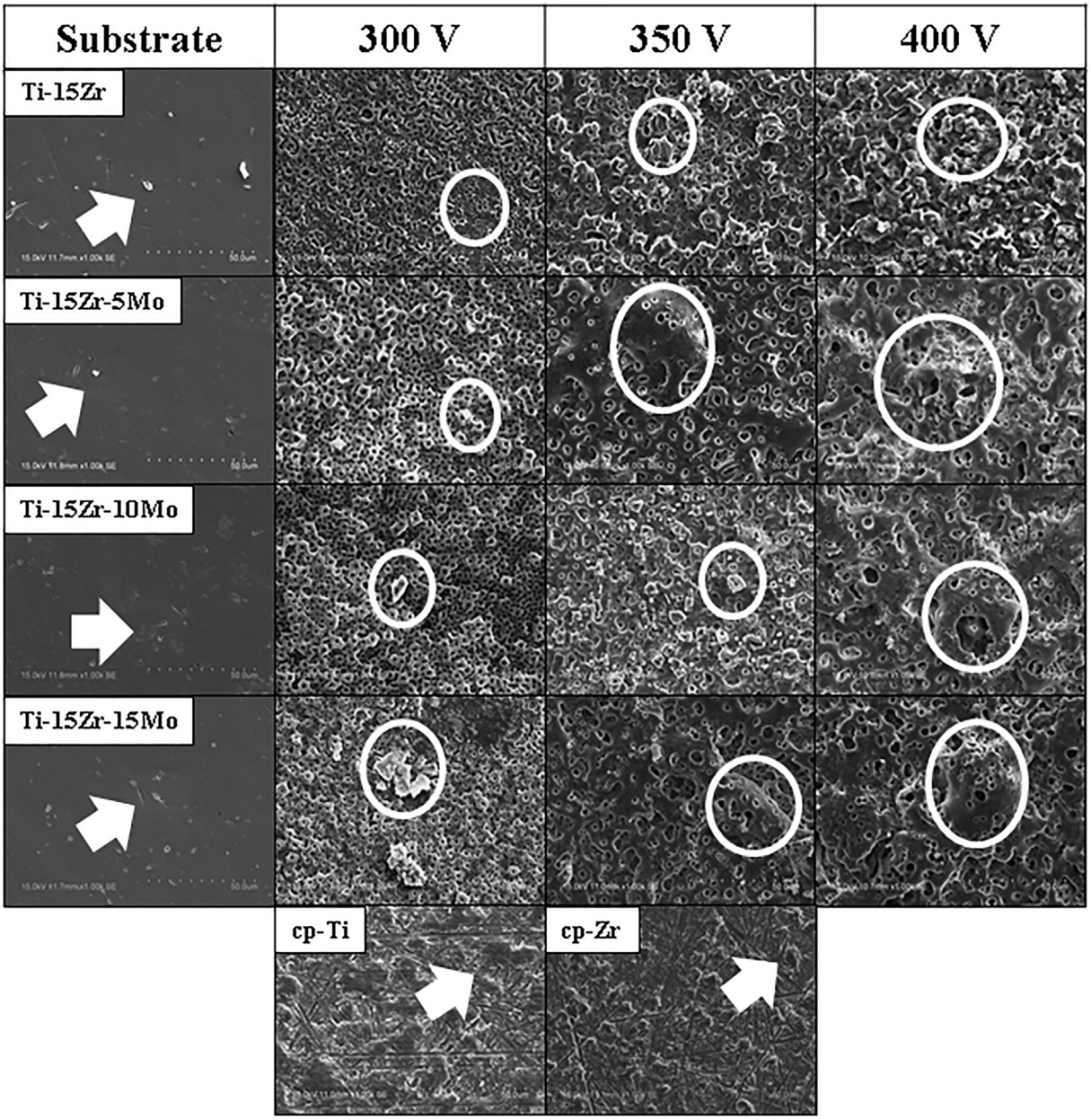

Fig. 7. Morphology of the samples after immersion in Hanks' solution for 7 days.

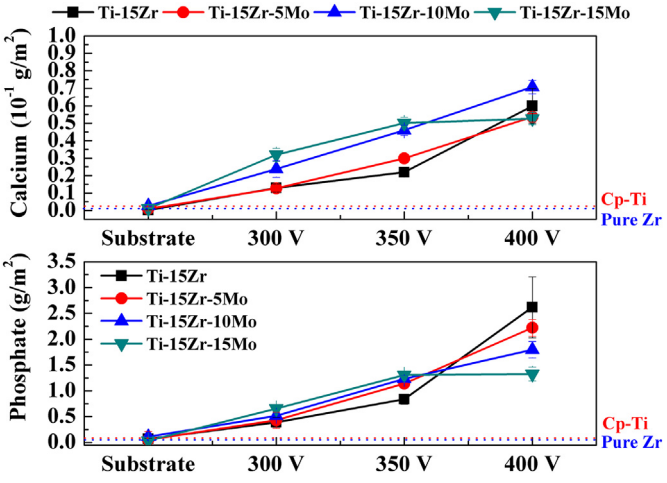

Fig. 8. Amount of calcium and phosphate ions in the immersed samples.

and traces of Mo oxides. From a crystalline point of view, the three distinct regions of the film are also shown. Firstly, a thin dense inner layer composed by amorphous phase originated from growth of the native passive film. Then, a crystalline layer composed by nanocrystals of anatase and rutile phases, created by oxidation reactions induced by the applied voltage. Finally, a thick amorphous outer layer formed during plasma sparking. It should be pointed out that the size and distribution of the amorphous and crystalline layers obtained in this study were distinct from those reported by Oliveira et al. [8] for cp-Ti. It indicates that not only MAO experimental parameters but also the alloy's composition plays important roles in the growth mechanism of MAO films.

Fig. 7 shows SEM images of the MAO-treated and untreated samples, together with cp-Ti and pure Zr, after immersion in Hanks' solution for 7 days. As expected, untreated samples did not exhibit a significant bioactive response, as only a few calcium phosphate precipitates were identified along the surface. On the other hand, a considerable group of precipitates grew at the MAO films. The films

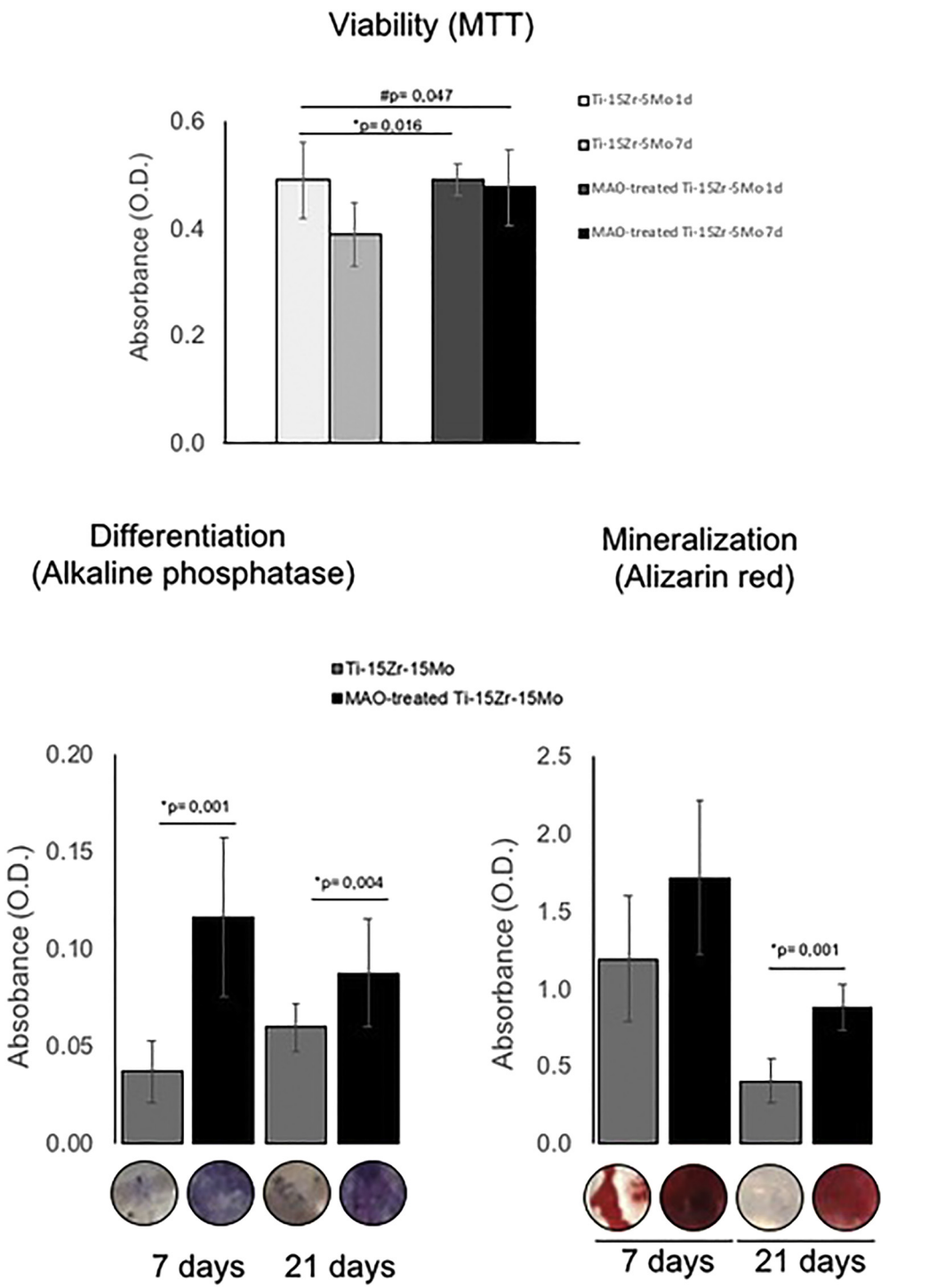

Fig. 9. Metabolic activity, alkaline phosphatase and alizarin activity of Saos-2 cultured on Ti-15Zr-15Mo as-cast and MAO-treated samples (400 V).

produced at higher voltages were almost covered with calcium phosphate on account of the Ca and P enrichment of the outer oxide layers. No differences were noted in the calcium phosphate precipitation as a function of the alloy's composition. Also, although the amount of calcium phosphate formation in the MAO films was lower in cp-Ti, it was still higher than that observed in pure Zr. This reduced formation of calcium phosphate precipitation on the MAO films, compared to a Ti surface, could be a result of the considerable amount of Zr in the oxide layer (as ZrO_2), which is recognized to hinder calcium phosphate formation [28]. The amount of calcium and phosphate ions evaluated by ICP-AES is shown in Fig. 8. The calcium and phosphate contents increased with the limiting voltage in all samples, due to the enrichment of the oxide layer with Ca and P atoms. MAO-treated samples presented higher amounts of precipitated ions compared to untreated samples. Despite the amount of calcium and phosphate ions detected could stem in part from the underlying oxide layers, the result indicates that a possible bioactive response was introduced by the MAO treatment.

In a similar study, Tsutsumi et al. [14] observed a calcium phosphate covering in MAO-treated Ti-29Nb-13Ta-4.6Zr alloy enriched with Ca and P ions, after 7 days of immersion in Hanks' solution. In another study, Ha et al. [29] obtained an improvement of the bioactive response

of Zr-based implants using MAO treatment in H_2SO_4 and NaOH solutions with constant current density of 188 A/m^2 for 10 min. Therefore, our results indicate that the Ca and P enrichment in the MAO film induced a possible bioactive response in the alloys.

The viability, differentiation and mineralization of human osteoblasts cell line (Saos-2) cultured on Ti-15Zr-15Mo as-cast and MAO treated samples was investigated and the results represented in Fig. 9. There were no significant differences on the metabolic activity of Ti-15Zr-15Mo MAO treated surfaces when compared to Ti-15Zr-15Mo as-cast, that was used as control, after 1 day of culture. However, after seven days of culture, a significant increase in the cellular metabolic activity was observed for Ti-15Zr-15Mo MAO treated surfaces, indicating that these surfaces induce cell proliferation throughout the culture time. Differentiation studies using the colorimetric assay of alkaline phosphatase (ALP) was carried out after 7 and 21 days of culture. As observed in Fig. 9, Saos-2 cultured on Ti-15Zr-15Mo MAO treated surfaces induce a significant increase of ALP activity indicating that this surface increase osteoblastic differentiation compared with the control, both at 7 and 21 days. This was confirmed by matrix mineralization studies (alizarin red assay) performed also at the same time of culture. A higher mineralization was observed for Saos-2 cultured in Ti-15Zr-15Mo MAO treated surface compared with Ti-15Zr-15Mo as-cast. This increase in mineralization was observed after 7 days but became significant after 21 days of culture. Saos-2 presents a mature osteoblasts phenotype [30], that mineralize quite fast, especially with high cell density, as reported in literature. It is possible that cells reach their maximum plateau of mineralization between 7 and 21 days. For higher culture time, cells proliferate, reaching a high confluence and start to detach from the surface, reducing the absorbance value, as observed in Fig. 9. The biocompatibility of titanium MAO treated surfaces was already reported in literature [31], however for the first time we demonstrate that Ti-15Zr-15Mo alloy is also suitable for the production of biocompatible oxide layers. The improved osteoblast viability, differentiation and mineralization of Ti-15Zr-15Mo MAO treated surface is the result of the surface topography, crystalline structure and chemical composition. It is possible that the enrichment of the oxide layer with Ca and P atoms together with a higher surface roughness and crystalline phases induce a higher osteoblast viability as well as mineralization. In addition, the porous structure might be suitable to improve the osseointegrative response through anchoring effect of bone tissue at the film [31].

4. Conclusion

MAO treatment was used to obtain bioactive surfaces in novel Ti-15Zr-xMo alloys developed for use as osseointegrative implants. All MAO films showed porous morphology with pore size and thickness < 4.5 μm and 15 μm, respectively, which were directly dependent of the limiting voltage. The MAO films exhibited low crystallinity, which was confirmed by the distinct amorphous and nanocrystalline regions observed by cross-sectional TEM analysis. Automated phase and orientation mapping confirmed that the MAO films were composed of inner and outer amorphous layers and an intermediary nanocrystalline region of mixed anatase and rutile phases. Ca atoms were located preferentially in the outer layer of the film. Immersion in Hanks' solution for 7 days showed that MAO-treated samples presented noticeable improvement in the bioactive response, despite the high amount of Zr in the oxide layer. Biological tests demonstrate that Ti-15Zr-xMo alloys and MAO-treated surfaces are biocompatible. Enhanced mineralization of human osteoblasts was observed in MAO-treated surfaces. These results suggest that the combined effect of textured surfaces and surface enrichment with Ca, P is a very promising approach to promote bone formation, suggesting an emerging application as osseointegrative implants.

Acknowledgements

The research was supported by Brazilian agencies funding CNPq (grant # 207417/2015-6), CAPES (grant # 99999.008666/2014-08) and FAPESP (grant # 00851-6/2015), and also by Japan Agency for Medical Research and Development (AMED), International Collaborative Research Program: Strategic International Research Cooperative Program (SICP), No. 16jm0310021h0004 and The Light Metal Educational Foundation, Inc. The authors are grateful to Gabriela Castro for the support in the biological assays. A. R. Ribeiro acknowledges the Jovem Cientista do Nosso Estado (2017) and PROPESQ-UNIGRANRIO/FUNADESP fellowships.

Author contributions

Correa, D.R.N. prepared the samples, conducted surface modifications and characterizations, and wrote the paper. Rocha, L.A. managed, planning and funding the project. Ribeiro, A.R. supported TEM and biological analysis. Gemini-Piperni, S. conducted cell vitality and proliferation analyses. Archanjo, B.S. prepared TEM samples by focused ion beam (FIB). Achete, C.A. managed and funded TEM analyses. Werckmann, J. conducted TEM analyses. Afonso, C.R.M. conducted automated phase and orientation mapping. Shimabukuro, M. supported surface modification and characterization. Doi, H. supported alloy casting, molding and characterization. Tsutsumi, Y. managed and supported surface modification and characterization. Hanawa, T. managed and funding the project. All authors discussed the results and reviewed the final manuscript.

References

[1] Y. Kirmanidou, M. Sidira, M.E. Drosou, V. Bennani, A. Bakopoulou, A. Tsouknidas, N. Michailidis, K. Michalakis, New Ti-alloys and surface modifications to improve the mechanical properties and the biological response to orthopedic and dental implants: a review, Biomed. Res. Int. 2016 (2016) 2908570.

[2] M. Niinomi, Y. Liu, M. Nakai, H. Liu, H. Li, Biomedical titanium alloys with Young's moduli close to that of cortical bone, Regen. Biomater. (2016), http://dx.doi.org/10.1093/rb/rbw016(2016) rbw016.

[3] D.R.N. Correa, F.B. Vicente, R.O. Araújo, M.L. Lourenço, P.A.B. Kuroda, M.A.R. Buzalaf, C.R. Grandini, Effect of the substitutional elements on the microstructure of the Ti-15Mo-Zr and Ti-15Zr-Mo systems alloys, J. Mater. Res. Technol. 4 (2015) 180–185.

[4] D.R.N. Correa, P.A.B. Kuroda, C.R. Grandini, L.A. Rocha, F.G.M. Oliveira, A.C. Alves, F. Toptan, Tribocorrosion behavior of β-type Ti-15Zr-based alloys, Mater. Lett. 179 (2016) 118–121.

[5] D. Duraccio, F. Mussano, M.G. Faga, Biomaterials for dental implants: current and future trends, J. Mater. Sci. 50 (2015) 4779–4812.

[6] X. Liu, P. Chu, C. Ding, Surface modification of titanium, titanium alloys, and related materials for biomedical applications, Mater. Sci. Eng. R. Rep. 47 (2004) 49–121.

[7] Y. Wang, H. Yu, C. Chen, Z. Zhao, Review of the biocompatibility of micro-arc oxidation coated titanium alloys, Mater. Des. 85 (2015) 640–652.

[8] F.G. Oliveira, A.R. Ribeiro, G. Perez, B.S. Archanjo, C.P. Gouvea, J.R. Araújo, A.P.C. Campos, A. Kuznetsov, C.M. Almeida, M.M. Maru, C.A. Achete, P. Ponthiaux, J.-P. Celis, L.A. Rocha, Understanding growth mechanisms and tribocorrosion behaviour of porous TiO_2 anodic films containing calcium, phosphorous and magnesium, Appl. Surf. Sci. 341 (2015) 1–12.

[9] A.R. Ribeiro, F. Oliveira, L.C. Boldrini, P.E. Leite, P. Falagan-Lotsch, A.B. Linhares, W.F. Zambuzzi, B. Fragneaud, A.P. Campos, C.P. Gouvea, B.S. Archanjo, C.A. Achete, E. Marcantonio Jr., L.A. Rocha, J.M. Granjeiro, Micro-arc oxidation as a tool to develop multifunctional calcium-rich surfaces for dental implant applications, Mater. Sci. Eng. C 54 (2015) 196–206.

[10] S.A. Alves, R. Bayón, A. Igartua, V. Saénz de Viteri, L.A. Rocha, Tribocorrosion behaviour of anodic titanium oxide films produced by plasma electrolytic oxidation for dental implants, Lubr. Sci. 26 (2014) 500–513.

[11] M. Sowa, M. Piotrowska, M. Widziolek, G. Dercz, G. Tylko, T. Gorewoda, A.M. Osyczka, W. Simka, Bioactivity of coatings formed on Ti-13Nb-13Zr alloy using plasma electrolytic oxidation, Mater Sci Eng C Mater Biol Appl 49 (2015) 159–173.

[12] A. Krząkała, K. Służalska, M. Widziołek, J. Szade, A. Winiarski, G. Dercz, A. Kazek, G. Tylko, J. Michalska, A. Iwaniak, A.M. Osyczka, W. Simka, Formation of bioactive coatings on a Ti–6Al–7Nb alloy by plasma electrolytic oxidation, Electrochim. Acta 104 (2013) 407–424.

[13] A. Kazek-Kęsik, G. Dercz, K. Suchanek, I. Kalemba-Rec, J. Piotrowski, W. Simka, Biofunctionalization of Ti–13Nb–13Zr alloy surface by plasma electrolytic oxidation. Part I, Surf. Coat. Technol. 276 (2015) 59–69.

[14] Y. Tsutsumi, M. Niinomi, M. Nakai, H. Tsutsumi, H. Doi, N. Nomura, T. Hanawa, Micro-arc oxidation treatment to improve the hard-tissue compatibility of Ti–29Nb–13Ta–4.6Zr alloy, Appl. Surf. Sci. 262 (2012) 34–38.
[15] H.P. Felgueiras, L. Castanheira, S. Changotade, F. Poirier, S. Oughlis, M. Henriques, C. Chakar, N. Naaman, R. Younes, V. Migonney, J.P. Celis, P. Ponthiaux, L.A. Rocha, D. Lutomski, Biotribocorrosion (tribo-electrochemical) characterization of anodized titanium biomaterial containing calcium and phosphorus before and after osteoblastic cell culture, J. Biomed. Mater. Res. B Appl. Biomater. 103 (2015) 661–669.
[16] Y. Tanaka, E. Kobayashi, S. Hiromoto, K. Asami, H. Imai, T. Hanawa, Calcium phosphate formation on titanium by low-voltage electrolytic treatments, J. Mater. Sci. Mater. Med. 18 (2007) 797–806.
[17] M. Nyan, Y. Tsutsumi, K. Oya, H. Doi, N. Nomura, S. Kasugai, T. Hanawa, Synthesis of novel oxide layers on titanium by combination of sputter deposition and micro-arc oxidation techniques, Dent. Mater. J. 30 (2011) 754–761.
[18] A.C. Alves, F. Oliveira, F. Wenger, P. Ponthiaux, J.P. Celis, L.A. Rocha, Tribocorrosion behaviour of anodic treated titanium surfaces intended for dental implants, J. Phys. D. Appl. Phys. 46 (2013) 404001.
[19] H.-T. Chen, C.-H. Hsiao, H.-Y. Long, C.-J. Chung, C.-H. Tang, K.-C. Chen, J.-L. He, Micro-arc oxidation of β-titanium alloy: structural characterization and osteoblast compatibility, Surf. Coat. Technol. 204 (2009) 1126–1131.
[20] Y.-L. Zhou, D.-M. Luo, Corrosion behavior of Ti–Mo alloys cold rolled and heat treated, J. Alloys Compd. 509 (2011) 6267–6272.
[21] M.-K. Han, M.-J. Hwang, M.-S. Yang, H.-S. Yang, H.-J. Song, Y.-J. Park, Effect of zirconium content on the microstructure, physical properties and corrosion behavior of Ti alloys, Mater. Sci. Eng. A 616 (2014) 268–274.
[22] B. Yang, Preparation of bioactive titanium metal via anodic oxidation treatment, Biomaterials 25 (2004) 1003–1010.
[23] W.F. Cui, C.J. Shao, The improved corrosion resistance and anti-wear performance of Zr–xTi alloys by thermal oxidation treatment, Surf. Coat. Technol. 283 (2015) 101–107.
[24] D.R. Lide, CRC Handbook of Chemistry and Physics, CRC Press, Boca Raton, FL, 2005.
[25] E.A. Ferreira, R.C. Rocha-Filho, S.R. Biaggio, N. Bocchi, Corrosion resistance of the Ti–50Zr at.% alloy after anodization in different acidic electrolytes, Corros. Sci. 52 (2010) 4058–4063.
[26] W. Simka, A. Krząkała, D.M. Korotin, I.S. Zhidkov, E.Z. Kurmaev, S.O. Cholakh, K. Kuna, G. Dercz, J. Michalska, K. Suchanek, T. Gorewoda, Modification of a Ti–Mo alloy surface via plasma electrolytic oxidation in a solution containing calcium and phosphorus, Electrochim. Acta 96 (2013) 180–190.
[27] D.P. Aun, M. Houmard, M. Mermoux, L. Latu-Romain, J.-C. Joud, G. Berthomé, V.T.L. Buono, Development of a flexible nanocomposite TiO_2 film as a protective coating for bioapplications of superelastic NiTi alloys, Appl. Surf. Sci. 375 (2016) 42–49.
[28] T. Hanawa, An overview of biofunctionalization of metals in Japan, J. R. Soc. Interface 6 (2009) 361–369.
[29] J.-Y. Ha, Y. Tsutsumi, H. Doi, N. Nomura, K.-H. Kim, T. Hanawa, Enhancement of calcium phosphate formation on zirconium by micro-arc oxidation and chemical treatments, Surf. Coat. Technol. 205 (2011) 4948–4955.
[30] C. Pautke, M. Schieker, T. Tischer, A. Kolk, P. Neth, W. Mutschler, S. Milz, Characterization of osteosarcoma cell lines MG-63, Saos-2 and U-2 OS in comparison to human osteoblasts, Anticancer Res. 24 (2004) 3743–3748.
[31] Y. Sul, The significance of the surface properties of oxidized titanium to the bone response: special emphasis on potential biochemical bonding of oxidized titanium implant, Biomaterials 24 (2003) 3893–3907.